

# Understanding the muon anomalous magnetic moment in light of a flavor symmetry-based Minimal Supersymmetric Standard Model

Mureed Hussain\* and Rizwan Khalid†

Department of Physics, School of Natural Sciences, National University of Sciences & Technology, H-12, Islamabad, Pakistan

## Abstract

We investigate whether the Minimal Supersymmetric Standard Model with the scalar masses of the third generation distinct from the first two, in order to be able to accommodate the muon anomalous magnetic moment, is consistent with the latest results from LHCb, direct collider bounds from ATLAS and CMS. In particular, we show that this class of models allows for satisfying both the constraints from the muon  $(g - 2)_\mu$  experiment and various bounds from the LHC. In addition, such models can also explain the observed dark matter relic density.

## 1 Introduction

Precision studies in B Physics provide a popular mechanism to constrain any scenario beyond the Standard Model (SM) in general [1, 2], and supersymmetry (SUSY) in particular [3–5]. With the Large Hadron Collider beauty (LHCb) experiment, we have entered a new era of precision measurement that puts increasingly stringent constraints on, for example, the Minimal Supersymmetric Standard Model (MSSM) [6–9]. Constraints from rare B decays like  $b \rightarrow s\gamma$ ,  $B_s \rightarrow \mu^+\mu^-$ ,  $B_u \rightarrow \tau\nu_\tau$  are routinely used in SUSY parametric space studies (see for example [10]). LHCb has also given quantum chromodynamics (QCD) form factor independent observables in connection with the semi-leptonic rare decay ( $B_d \rightarrow K^*\mu^+\mu^-$ ) [11]. An important result for this decay is the zero crossing value of the forward-backward asymmetry ( $\mathcal{A}_{FB}$ ),

$$q_0^2 = 4.9 \pm 0.9 \text{ (GeV}^2\text{)} \quad (1)$$

In addition, a host of form factor independent observables related to transversity amplitudes in the  $B_d \rightarrow K^*\mu^+\mu^-$  decay are now known experimentally (see Section 2 for details). So far, B physics constraints do not imply any significant deviation from the SM, and, therefore, set a lower bound on any new physics.

The SM prediction for the anomalous magnetic moment of the muon,  $a_\mu = (g - 2)_\mu/2$  (hereafter referred to as the  $g_\mu - 2$  anomaly) [12], has a  $3.5\sigma$  discrepancy with the experimental

---

\*Email: mureed.hussain@sns.nust.edu.pk

†Email: rizwan@sns.nust.edu.pk

results [13]. If new physics is to offer a solution to this discrepancy, then this discrepancy provides both an upper and a lower bound for it. This is, of course, also true for low scale supersymmetry [14]. It is an interesting question to probe whether the  $g_\mu - 2$  anomaly can be resolved given that we also simultaneously satisfy the constraints from direct searches for SUSY particles and indirect probes via B physics.

The discovery of the Higgs boson with a mass  $\sim 125$  GeV [15, 16] has important consequences, in general, for low scale supersymmetry. In the MSSM such a heavy Higgs mass requires either a large,  $\mathcal{O}(\text{few} - 10)$  TeV stop squark mass, or alternatively, a relatively large soft supersymmetry breaking (SSB) trilinear  $A_t$ -term, along with a stop squark mass of around a TeV [17]. The constraints coming from the Higgs boson mass are particularly stringent regarding the sparticle spectrum if we assume universal boundary conditions on the soft SUSY breaking (SSB) parameters at some high energy scale (typically  $M_{GUT} \sim 10^{16} \text{GeV}$ ). Such universal boundary conditions for the SSB terms are well motivated in minimal scenarios of gravity [18] or gauge mediation [19]. For instance, in the simple version of gravity or gauge mediation scenarios with universal scalar and gaugino mass terms, it is difficult to simultaneously explain the observed Higgs boson mass and resolve the  $g_\mu - 2$  anomaly. There have been several recent attempts to reconcile this presumed tension between the muon  $g_\mu - 2$  and the 125 GeV Higgs mass [20].

In this paper we use the framework of flavor symmetry based Minimal Supersymmetric Standard Model (sMSSM) suggested recently [21, 22], consisting of seven phenomenological parameters which describe SUSY breaking. We show that it is possible to explain the  $g_\mu - 2$  anomaly and the Higgs boson mass simultaneously, along with the observed dark matter abundance in addition to satisfying direct mass bounds on sparticles and constraints from LHCb. In doing so, we follow the approach of [21]. However, we have incorporated the constraints from the  $B_d \rightarrow K^* \mu^+ \mu^-$  channel which were not studied in [21] and in addition, we have used updated values of all constraints.

In Section 2 we give the effective theory concerning semi-leptonic weak decays and discuss several experimental observables that we incorporate in our study. In Section 3 we give details of the sMSSM parameters along with our scanning procedure and constraints. In Section 4 we discuss our results after which we conclude in Section 5.

## 2 Effective Theory of semi-leptonic B decays

Despite being successful probes of new physics, the decays  $b \rightarrow s\gamma$ ,  $B_s \rightarrow \mu^+ \mu^-$  and  $B_u \rightarrow \tau \nu_\tau$  have a small number of observables like CP asymmetries and branching ratios. The constraints on MSSM from the branching ratio of  $b \rightarrow s\gamma$  and its time dependent CP asymmetries are studied in [23–25]. The rare decay  $B_s \rightarrow \mu^+ \mu^-$  which is helicity suppressed in the SM and so contributes by additional diagrams in the MSSM is also used for constraining the MSSM parameter space as in [3, 26, 27]. The rare decay  $B_d \rightarrow K^* \mu^+ \mu^-$  provides along with the differential branching ratio as a function of square of the dilepton invariant mass ( $q^2$ ), observables such as  $K^*$  longitudinal polarization fraction ( $F_L$ ) and forward-backward asymmetry ( $\mathcal{A}_{FB}$ ), where

$$F_L = \frac{\Gamma_L}{\Gamma} ,$$

$$\mathcal{A}_{FB} = \frac{N_F - N_B}{N_F + N_B} . \quad (2)$$

$\Gamma_L$  is the decay rate of  $B_d \rightarrow K^* \mu^+ \mu^-$  when  $K^*$  is longitudinally polarized and  $\Gamma$  is the total decay rate. Likewise,  $N_F$  is the number of events in which  $\mu^-(\mu^+)$  is moving in the *forward*

direction with respect to  $B_d(\bar{B}_d)$  in the dilepton rest frame, and  $N_B$  is the corresponding number of events in the *backward* direction. In terms of the differential cross-section  $\frac{d\sigma}{d\Omega}$ ,  $\mathcal{A}_{FB}$  is given as;

$$\mathcal{A}_{FB} = \frac{\int_0^\pi d\Omega \frac{d\sigma}{d\Omega} - \int_{-\pi}^0 d\Omega \frac{d\sigma}{d\Omega}}{\int_{-\pi}^\pi d\Omega \frac{d\sigma}{d\Omega}} \quad (3)$$

In addition, the zero crossing of this  $\mathcal{A}_{FB}$  given in Eq. 1 is also important as it puts constraints on a variety of models [28].

Semi-leptonic part of the effective Hamiltonian which is most sensitive to the  $b \rightarrow s\ell\ell$  [29,30] decay is composed of radiative and dileptonic operators and is given by

$$\mathcal{H}_{\text{eff}}^{\text{sl}} = -\frac{4G_F}{\sqrt{2}} V_{tb} V_{ts}^* \left[ \sum_{i=7,9,10} (\mathcal{C}_i \mathcal{O}_i + \mathcal{C}'_i \mathcal{O}'_i) + \sum_{i=1,2} (\mathcal{C}_{\mathcal{Q}_i} \mathcal{Q}_i + \mathcal{C}'_{\mathcal{Q}_i} \mathcal{Q}'_i) \right], \quad (4)$$

where the operators  $\mathcal{O}_i$  and  $\mathcal{Q}_i$  in  $\mathcal{H}_{\text{eff}}^{\text{sl}}$  are,

$$\begin{aligned} \mathcal{O}'_7 &= (\frac{e}{16\pi^2}) m_b [\bar{s} \sigma^{\mu\nu} P_{R(L)} b] F_{\mu\nu}, \quad \mathcal{O}'_9 = (\frac{e^2}{16\pi^2}) [\bar{s} \gamma^\mu P_{L(R)} b] [\bar{\ell} \gamma_\mu \ell], \\ \mathcal{O}'_{10} &= (\frac{e^2}{16\pi^2}) m_b [\bar{s} \gamma^\mu P_{L(R)} b] [\bar{\ell} \gamma_\mu \gamma_5 \ell], \\ \mathcal{Q}'_1 &= (\frac{e^2}{16\pi^2}) m_b [\bar{s} P_{R(L)} b] [\bar{\ell} \ell], \quad \mathcal{Q}'_2 = (\frac{e^2}{16\pi^2}) m_b [\bar{s} P_{R(L)} b] [\bar{\ell} \gamma_5 \ell]. \end{aligned} \quad (5)$$

The four-body final state ( $B \rightarrow K^* \ell^+ \ell^-$  (where  $K^* \rightarrow K\pi$ )) differential decay distribution provides a variety of experimental constraints. This differential decay distribution depends on the following kinematic variables:

- $q^2$ : The invariant mass square of lepton.
- $\theta_\ell$ : Angle between the directions of flight of the  $\ell^+(\ell^-)$  and the  $B$  meson in the dilepton rest frame.
- $\theta_K$ : Angle between directions of flight of kaon ( $K$ ) and the  $B$  meson in the rest frame of  $K^*$ .
- $\phi$ : The azimuthal angle between the planes of lepton pair and the  $K\pi$  system.

In terms of these kinematic variables, the differential decay rate is

$$\begin{aligned} \frac{d^4\Gamma(B_d)}{dq^2 d\cos\theta_K d\cos\theta_\ell d\phi} &= \frac{9}{32\pi} [J_{1s} \sin^2 \theta_K + J_{1c} \cos^2 \theta_K + (J_{2s} \sin^2 \theta_K + J_{2c} \cos^2 \theta_K) \cos 2\theta_\ell \\ &\quad + J_3 \sin^2 \theta_K \sin^2 \theta_\ell \cos 2\phi + J_4 \sin 2\theta_K \sin 2\theta_\ell \cos \phi \\ &\quad + J_5 \sin 2\theta_K \sin \theta_\ell \cos \phi + (J_{6s} \sin^2 \theta_K + J_{6c} \cos^2 \theta_K) \cos \theta_\ell \\ &\quad + J_7 \sin 2\theta_K \sin \theta_\ell \sin \phi + J_8 \sin 2\theta_K \sin 2\theta_\ell \sin \phi \\ &\quad + J_9 \sin^2 \theta_K \sin^2 \theta_\ell \sin 2\phi]. \end{aligned} \quad (6)$$

The coefficients  $J_i$  depend on the transversity amplitudes (decay amplitudes in which the particles' spins are projected normal to the reaction plane) and their explicit form is given in [31]. The fully accessible phase space is bounded from the kinematics by

$$4m_{\ell^2} \leq q^2 \leq (M_B - m_{K^*})^2, \quad -1 \leq \cos \theta_\ell \leq 1, \quad -1 \leq \cos \theta_K \leq 1, \quad 0 \leq \phi \leq 2\pi.$$

These  $J_i(q^2)$  integrated in different  $q^2$  bins form the basic observables for this decay. To minimize the hadronic uncertainties some optimized (form factor independent) observables can be constructed by taking appropriate ratios of these  $J_i$ 's. All of these observables from  $B_d \rightarrow K^* \mu^+ \mu^-$  can be measured at the LHCb as a function of  $q^2$  and this decay proves to be very important one for constraining the new physics scenarios [32]. The optimized observables denoted as  $P_i$  are,

$$\begin{aligned} \langle P_1 \rangle_{\text{bin}} &= \frac{1}{2} \frac{\int_{\text{bin}} dq^2 [J_3 + \bar{J}_3]}{\int_{\text{bin}} dq^2 [J_{2s} + \bar{J}_{2s}]}, & \langle P_2 \rangle_{\text{bin}} &= \frac{1}{8} \frac{\int_{\text{bin}} dq^2 [J_{6s} + \bar{J}_{6s}]}{\int_{\text{bin}} dq^2 [J_{2s} + \bar{J}_{2s}]}, \\ \langle P'_4 \rangle_{\text{bin}} &= \frac{1}{\mathcal{N}'_{\text{bin}}} \int_{\text{bin}} dq^2 [J_4 + \bar{J}_4], & \langle P'_5 \rangle_{\text{bin}} &= \frac{1}{2\mathcal{N}'_{\text{bin}}} \int_{\text{bin}} dq^2 [J_5 + \bar{J}_5], \\ \langle P'_6 \rangle_{\text{bin}} &= \frac{-1}{2\mathcal{N}'_{\text{bin}}} \int_{\text{bin}} dq^2 [J_7 + \bar{J}_7], & \langle P'_8 \rangle_{\text{bin}} &= \frac{1}{\mathcal{N}'_{\text{bin}}} \int_{\text{bin}} dq^2 [J_8 + \bar{J}_8], \end{aligned}$$

where  $\bar{J}_i$  correspond to the decay  $\bar{B} \rightarrow \bar{K}^* \mu^- \mu^+$  and the normalization factor is

$$\mathcal{N}'_{\text{bin}} = \sqrt{- \int_{\text{bin}} dq^2 [J_{2s} + \bar{J}_{2s}] \int_{\text{bin}} dq^2 [J_{2c} + \bar{J}_{2c}]}.$$

A comprehensive study of this preferable choice of observables in light of results from LHCb has been done in [33].

### 3 Flavor symmetry-based MSSM parameter space, Scanning Procedure and Constraints

We use the flavor symmetry-based MSSM (sMSSM) described in [22] as the basis of our study. In the sMSSM model, the SSB Lagrangian is consistent with two symmetries (a) a GUT symmetry such as  $S(10)$  and (b) a non-abelian flavor symmetry of gauge origin that acts on the three families with either a **2+1** or a **3** family assignment. The GUT scale symmetry reduces the MSSM parameters, for example, for gauginos the  $S(10)$  symmetry reduces the number of parameters from three to one. It also suggests that all members of a family would have a common soft mass, as they are unified into a **16**-plet of  $S(10)$ .

The non-abelian flavor symmetry suppresses the SUSY mediated flavor changing neutral current (FCNC) processes mediated by SUSY particles. This FCNC suppression is required here as we want our model to be compatible with GUT and also have different masses for the sfermions families. Any symmetry like  $SU(2)_f$  which has a doublet representation can be used as flavor symmetry but such symmetry will contain new sources of flavor violation, arising from the  $D$ -terms which split the masses of superparticles within a given multiplet after SUSY breaking [34]. An interchange symmetry has been suggested [22] that would set these  $D$ -terms to zero. So, for the flavor symmetry  $SU(2)_f$ , soft masses of the scalars for the 1<sup>st</sup> and 2<sup>nd</sup> family are in a doublet under  $SU(2)_f$  ( $(16_1, 16_2)$ ) while the third family is a singlet ( $16_3$ ) under  $SU(2)_f$ .

Together these two symmetries reduce the 15 soft squared mass parameters of the 15 chiral sfermions of the MSSM to just two. We consider the SUSY phenomenology of sMSSM to be described by seven parameters

$$m_{1,2}, m_3, M_{1/2}, A_0, \tan\beta, m_{H_u}, m_{H_d} \quad (7)$$

where  $m_{1,2}$  is the common mass parameter of first two family sfermions,  $m_3$  is the mass parameter of third family sfermions,  $M_{1/2}$  is the unified gaugino mass parameter,  $A_0$  is the unified trilinear coupling parameter, and  $\tan \beta$  is the ratio of the vacuum expectation values of the two Higgs doublets. Finally,  $m_{H_u}$  and  $m_{H_d}$  are the corresponding Higgs mass parameters for the two Higgs doublets which are set separately from any sfermions mass parameters. We employ the SOFTSUSY-3.5.2 package [35], which calculates the sparticle spectrum in the CP-conserving MSSM with a full flavor mixing structure to perform the random scans over the parametric space. This program solves the renormalization group equations with boundary conditions on the SSB terms specified at  $M_{GUT}$ . Weak scale gauge couplings and fermion mass data are used as a boundary condition at  $M_Z$  (the Z boson mass). The sMSSM parametric space that we have scanned is,

$$\begin{aligned}
0 &\leq m_{1,2} \leq 3000 \text{ GeV}, \\
0 &\leq m_3 \leq 3000 \text{ GeV}, \\
0 &\leq M_{1/2} \leq 3000 \text{ GeV}, \\
-3 &\leq A_0/m_3 \leq 3 \text{ GeV}, \\
-5000 &\leq A_0 \leq 5000 \text{ GeV}, \\
0 &\leq \tan \beta \leq 60 \text{ GeV}, \\
0 &\leq m_{H_u} \leq 5000 \text{ GeV}, \\
0 &\leq m_{H_d} \leq 5000 \text{ GeV}, \\
\mu &> 1.
\end{aligned} \tag{8}$$

In other words, we basically consider the parametric space of the non-universal Higgs model of type II (NUHM-II) [36], having independent parameters for up-type and down-type Higgs  $m_{H_u}$  and  $m_{H_d}$ , but with split masses of sfermions. Later in this article we will also discuss the scan over the parametric space of NUHM-I in which these two Higgs mass parameters are set equal to each other.

After the generation of SUSY LesHouches Accord (SLHA) [37] file via SOFTSUSY and hence the sparticle spectrum, we use the SUPERISO package [38] to calculate different B Physics observables.

Branching ratios of the  $B$  decays  $B_s \rightarrow \mu^+\mu^-$ ,  $b \rightarrow s\gamma$  and  $B_u \rightarrow \tau\nu_\tau$  have been used to constrain the parametric space of different MSSM models [23–27]. LHC also provides lower bounds on masses of the gluino and squarks [39, 40]. The Muon g-2 Collaboration [41] provides a significantly precise value of the anomalous magnetic moment of the muon. The difference between the experimental value of  $g_\mu - 2$  anomaly and its theoretical value calculated in the Standard Model is defined as  $\Delta a_\mu = a_\mu^{\text{exp}} - a_\mu^{\text{SM}}$ .

We apply these constraints along with constraints on the SM-like Higgs boson mass, on the parametric space of sMSSM as done in [21]. These constraints are

$$\left. \begin{aligned}
0.8 \times 10^{-9} &\leq BR(B_s \rightarrow \mu^+\mu^-) \leq 6.2 \times 10^{-9}, \\
2.99 \times 10^{-4} &\leq BR(b \rightarrow s\gamma) \leq 3.87 \times 10^{-4}, \\
0.15 &\leq \frac{BR(B_u \rightarrow \tau\nu_\tau)_{\text{MSSM}}}{BR(B_u \rightarrow \tau\nu_\tau)_{\text{SM}}} \leq 2.41,
\end{aligned} \right\} \tag{9}$$

$$\left. \begin{aligned}
m_{\tilde{g}} &\gtrsim 1550.0 \text{ GeV} \quad (m_{\tilde{g}} \sim m_{\tilde{q}}) \\
m_{\tilde{g}} &\gtrsim 1150.0 \text{ GeV} \quad (m_{\tilde{g}} \approx m_{\tilde{q}}) \\
m_{\tilde{q}} &\gtrsim 875.0 \text{ GeV}
\end{aligned} \right\} \tag{10}$$

$$20.8 \times 10^{-10} < \Delta a_\mu < 36.8 \times 10^{-10}, \tag{11}$$

$$123.0 \leq m_{h^0} \leq 127.0, \tag{12}$$

Finally, we apply constraints from optimized observables,  $P'_i$ s, of  $B_d \rightarrow K^* \mu^+ \mu^-$  given in Section 2 along with constraints from the zero crossing of  $\mathcal{A}_{FB}$  whose numerical value is given in Eq. (1).

## 4 Results

We next present our results of the scan over the parametric space given in Eq. (8). We now discuss our results for the NUHM-II type sMSSM.

### 4.1 sMSSM with NUHM-II

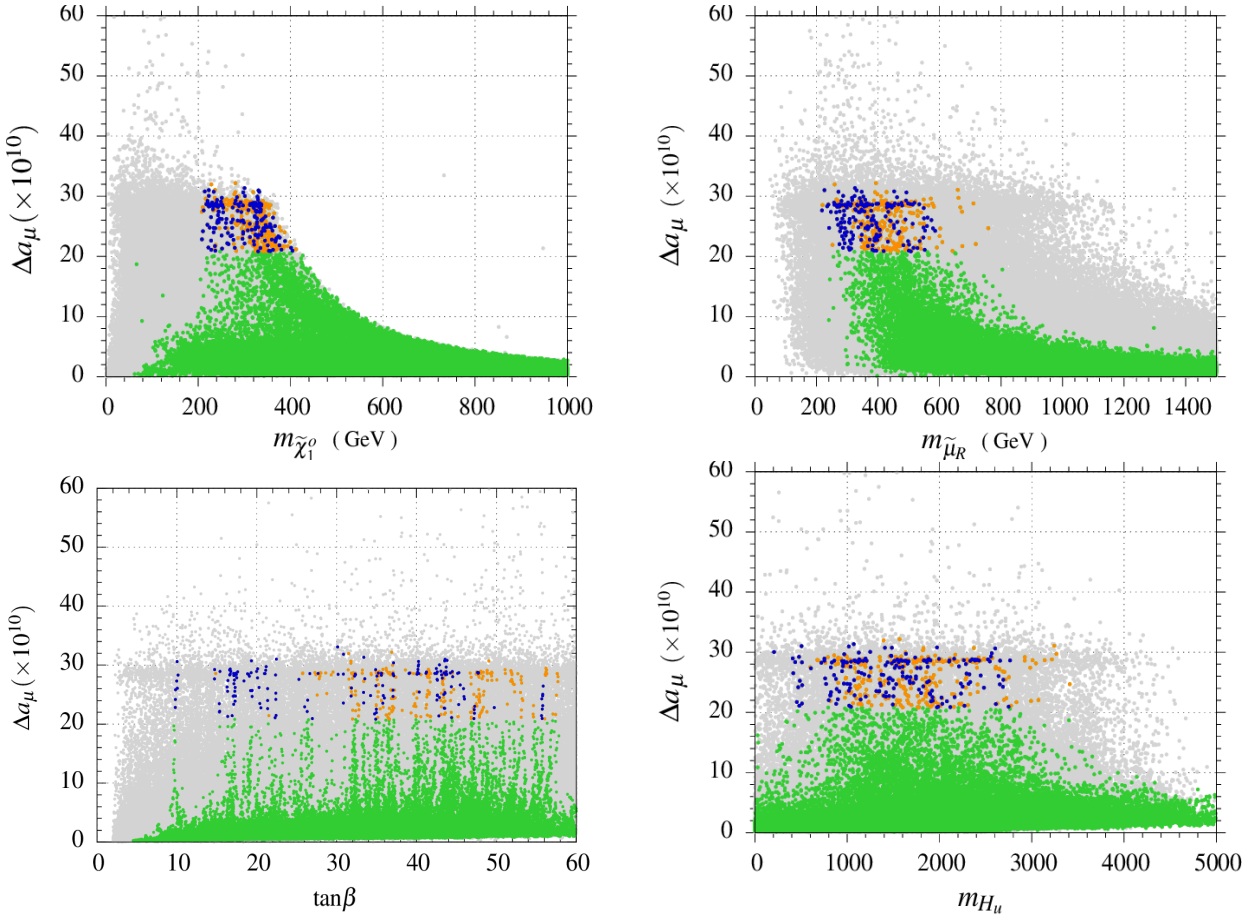


**Fig. 1.** All points satisfy the REWSB and neutralino LSP conditions. Green points form a subset of grey points and satisfy the B Physics constraints from  $BR(b \rightarrow s\gamma)$ ,  $BR(B_s \rightarrow \mu^+ \mu^-)$  and  $BR(B_u \rightarrow \tau \nu_\tau)$  along with Higgs, gluino and squark mass bounds. Orange points are a subset of green points and lie within the 1- $\sigma$  allowed range of the  $g_\mu - 2$  anomaly. Blue points form a subset of orange points and they satisfy B Physics constraints from  $B_d \rightarrow K^* \mu^+ \mu^-$  including zero crossing of  $\mathcal{A}_{FB}$  and seven other constraints, on optimized observables  $P'_i$ s, as given in [30].

In Fig. 1, we present results in the  $\Delta a_\mu - m_{\tilde{\chi}_1^0}$ ,  $\Delta a_\mu - m_{\tilde{\mu}_R}$ ,  $\Delta a_\mu - \tan \beta$  and  $\Delta a_\mu - m_{H_u}$  planes.  $m_{\tilde{\chi}_1^0}$  is the mass of the lightest neutralino,  $m_{\tilde{\mu}_R}$  is the mass of the SUSY partner of right handed muon. Grey points are consistent with radiative electroweak symmetry breaking (REWSB)



and these points also satisfy the condition of the neutralino being the lightest supersymmetric particle (LSP).

Green points form a subset of grey points and satisfy the B Physics constraints given in Eq. (9). Green points also satisfy the Higgs, gluino and squark mass constraints given in Eq. (10) and Eq. (12). Orange points are the subset of green points that satisfy the  $g_\mu - 2$  constraints given in Eq. (11). Blue points form a subset of orange points and satisfy the additional B Physics constraints given in Eq. (1) and seven other constraints on the optimized observables  $P_i$ 's, given in [30].

We can, from the  $\Delta a_\mu - m_{\tilde{\chi}_1^0}$  plane in Fig. 1, infer that in order to explain away the  $g_\mu - 2$  anomaly, the neutralino should be heavier than 150 GeV and lighter than 400 GeV. This range is also consistent with the constraints from  $B_d \rightarrow K^* \mu^+ \mu^-$  in addition to all the other constraints mentioned in Equations (9) to (12). In the  $\Delta a_\mu - m_{\tilde{\mu}_R}$  plane of Fig. 1, we find the mass of  $\tilde{\mu}_R$  to be in the range  $200 \text{ GeV} \lesssim m_{\tilde{\mu}_R} \lesssim 760 \text{ GeV}$  from the muon  $g_\mu - 2$ . An additional reduction of 160 GeV in the upper bound occurs due to constraints from  $B_d \rightarrow K^* \mu^+ \mu^-$ .

From results in the  $\Delta a_\mu - \tan \beta$  plane of Fig. 1, we see that  $\tan \beta \sim 10$  is the start of the allowed region from the  $g_\mu - 2$  constraint. It is also interesting to see that for  $\tan \beta \leq 27$ , the constraining regions from  $B \rightarrow K^* \mu^+ \mu^-$  and  $g_\mu - 2$  are almost overlapping. For higher  $\tan \beta$ , density of points that satisfy  $B \rightarrow K^* \mu^+ \mu^-$  decreases due to suppression via loop contributions of heavier sparticles which are  $\tan \beta$  dependent. The  $\Delta a_\mu - m_{H_u}$  plane of Fig. 1 shows that  $m_{H_u} \leq 3500 \text{ GeV}$  is in agreement with constraints from  $g_\mu - 2$ , B Physics (excluding those from  $B_d \rightarrow K^* \mu^+ \mu^-$ ), Higgs, gluino and sparticle masses given in Eq. (11), Eq. (9), Eq. (10) and Eq. (12), respectively. The constraints from  $B_d \rightarrow K^* \mu^+ \mu^-$  reduce this upper bound to  $\sim 2800 \text{ GeV}$ .

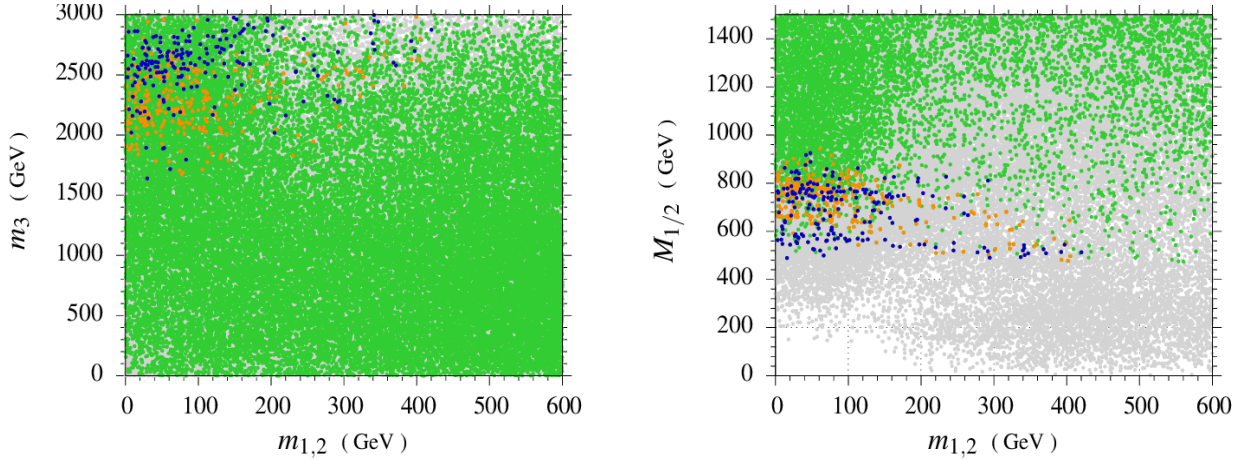


**Fig. 2.** Plots in  $m_3 - m_{1,2}$  and  $M_{1/2} - m_{1,2}$  planes. Color coding is the same as in Fig. 1. Clearly CMSSM( $m_{1,2} = m_3$ ) is ruled out by  $g_\mu - 2$  constraint.

In Fig. 2,  $m_3 - m_{1,2}$  plane, we can see that in order to satisfy the  $g_\mu - 2$  constraint along with other bounds,  $m_3/m_{1,2} \gtrsim 6$ . This is because a heavy  $m_3$  is needed to satisfy, for example, the Higgs mass bound and direct collider bounds on the stop. Likewise, a relatively small  $m_{1,2}$  ensures that the smuon and tau sneutrino are not too heavy and can contribute to the muon  $g_\mu - 2$ . We can see that in order to satisfy the  $g_\mu - 2$  constraint, the upper bound on  $m_{1,2}$  is 420 GeV and for that the lower bound on  $m_3$  is  $\sim 2850 \text{ GeV}$ . Since the  $g_\mu - 2$  constraint requires gauginos (bino or wino) to be lighter, we present our results in the  $M_{1/2} - m_{1,2}$  plane of Fig. 2. Gaugino masses are unified in our model (given by one parameter “ $M_{1/2}$ ”) and they are restricted to 900 GeV from both the  $g_\mu - 2$  anomaly constraint.

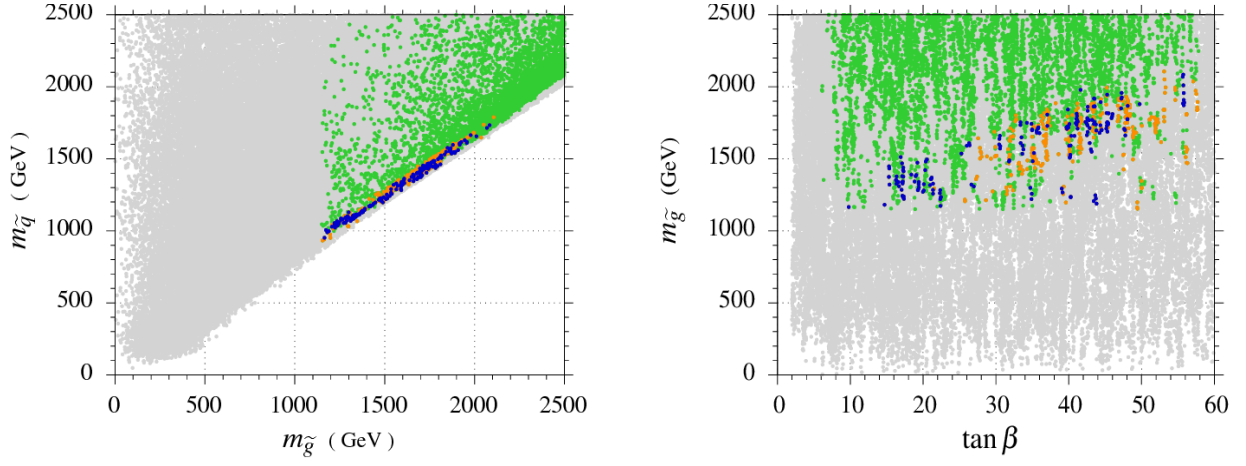


**Fig. 3.** Plots in the  $m_{\tilde{q}} - m_{\tilde{g}}$  and  $m_{\tilde{g}} - \tan \beta$  planes, color coding is the same as in Fig. 1.

We plot the gluino mass  $m_{\tilde{g}}$  versus  $m_{\tilde{q}}$  (the lightest of the first two generation squarks) in the left panel of Fig. 3. We show that there is an upper bound on the light squark masses  $\sim 1850$  GeV which arises from the fact that the contribution from the smuon is important for resolving the muon  $g_{\mu} - 2$  anomaly in the MSSM. Likewise, the lower bound is imposed by the direct mass bounds on  $m_{\tilde{q}}$  coming from LHC. Plot in the  $m_{\tilde{g}} - \tan \beta$  plane of Fig. 3 shows that  $\tan \beta \lesssim 10$  is not allowed, mainly because of the Higgs boson mass bounds. The upper limit on  $m_{\tilde{g}}$  for our chosen model is  $\sim 2100$  GeV.

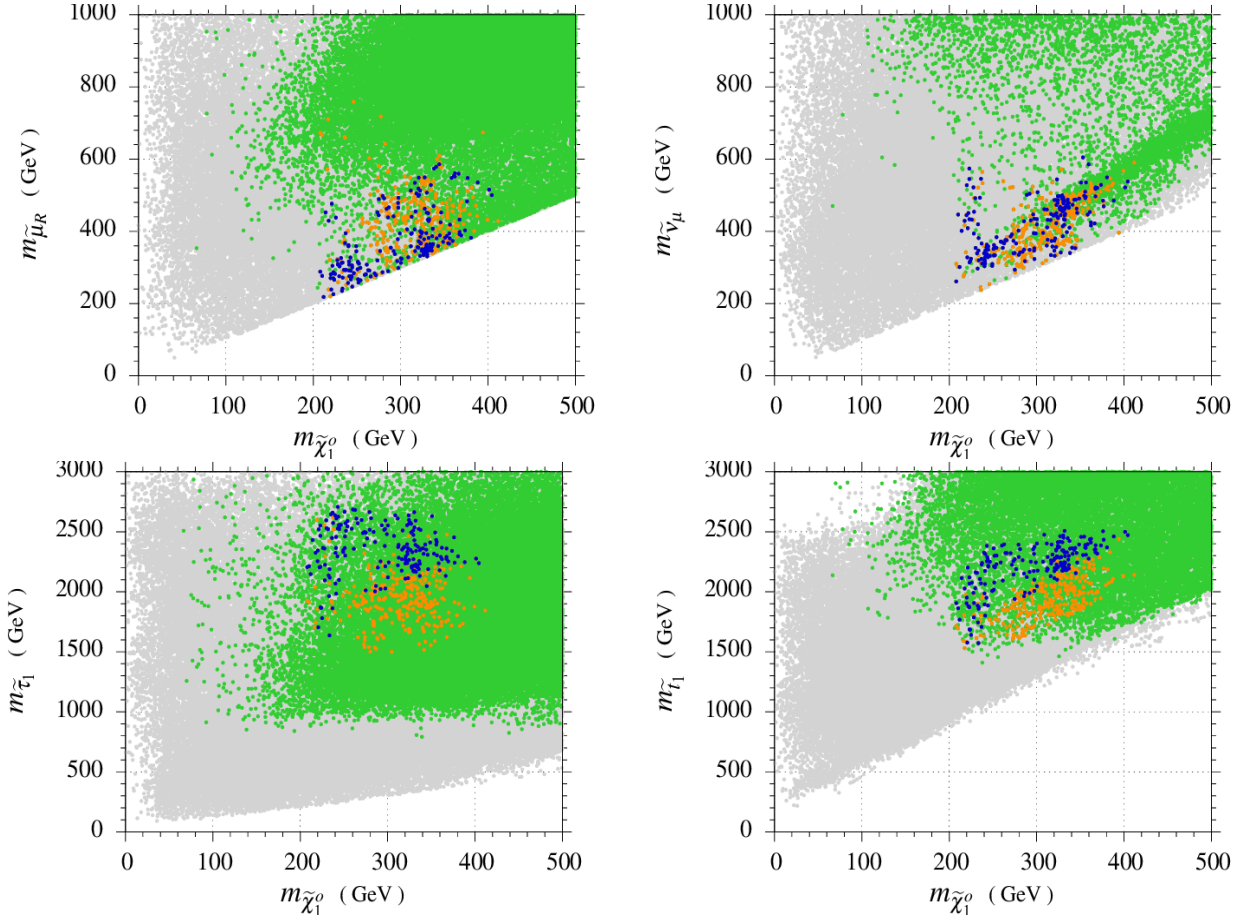


**Fig. 4.** Plots in the  $m_{\tilde{\mu}_R} - m_{\tilde{\chi}_1^0}$ ,  $m_{\tilde{\nu}_\mu} - m_{\tilde{\chi}_1^0}$ ,  $m_{\tilde{\tau}_1} - m_{\tilde{\chi}_1^0}$ ,  $m_{\tilde{t}_1} - m_{\tilde{\chi}_1^0}$  planes, color coding is the same as in Fig. 1.



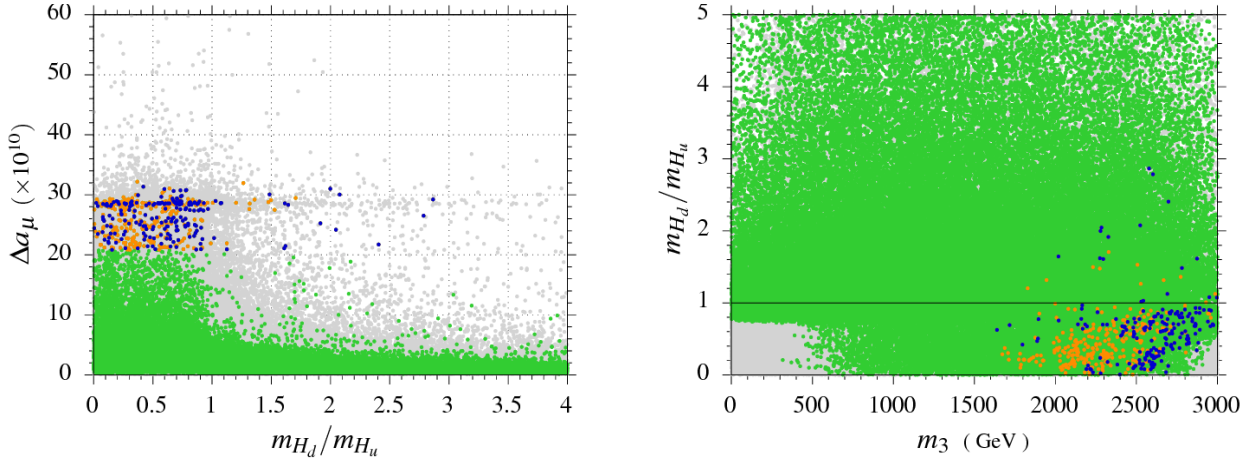


**Fig. 5.** Plots in the  $\Delta a_\mu - m_{H_d}/m_{H_u}$  and  $m_{H_d}/m_{H_u} - m_3$  planes, color coding is the same as in Fig. 1.

Next, in Fig. 4, we show our results in the  $m_{\tilde{\mu}_R} - m_{\tilde{\chi}_1^0}$ ,  $m_{\tilde{\nu}_\mu} - m_{\tilde{\chi}_1^0}$ ,  $m_{\tilde{\tau}_1} - m_{\tilde{\chi}_1^0}$  and  $m_{\tilde{t}_1} - m_{\tilde{\chi}_1^0}$  planes, where  $m_{\tilde{\nu}_\mu}$  is the mass of the SUSY partner of muon neutrino,  $m_{\tilde{\tau}_1}$  is the mass of the SUSY partner of tauon and  $m_{\tilde{t}_1}$  is the mass of the SUSY partner of top quark. We see that co-annihilation scenarios involving the smuon and muon sneutrino are compatible with the  $1-\sigma$  range of  $g_\mu - 2$  and also with constraints from  $B_d \rightarrow K^* \mu^+ \mu^-$ , so we expect the possibility of neutralino dark matter. This co-annihilation occurs in the neutralino mass range from 160 GeV to nearly 420 GeV<sup>1</sup>.

We can see from Fig. 4 that the  $B_d \rightarrow K^* \mu^+ \mu^-$  results play a crucial role in constraining the parameter space that is otherwise available. From the  $m_{\tilde{\mu}_R} - m_{\tilde{\chi}_1^0}$  plane we see that the upper bound on  $m_{\tilde{\mu}_R}$  is  $\sim 600$  GeV. In  $m_{\tilde{\nu}_\mu} - m_{\tilde{\chi}_1^0}$  plane we see that  $B_d \rightarrow K^* \mu^+ \mu^-$  constraints limit the upper bound on the  $m_{\tilde{\nu}_\mu}$  to  $\sim 650$  GeV. We see in the  $m_{\tilde{\tau}_1} - m_{\tilde{\chi}_1^0}$  plane that the  $B_d \rightarrow K^* \mu^+ \mu^-$  constraints shift up the lower bound on  $m_{\tilde{\tau}_1}$  of 1500 GeV from  $g_\mu - 2$ , by a 100 GeV while the upper bound is consistent with the  $g_\mu - 2$  which is  $\sim 2700$  GeV. As for the  $m_{\tilde{t}_1} - m_{\tilde{\chi}_1^0}$  plane, we see that the lower and upper bounds on  $m_{\tilde{t}_1}$  are  $\sim 1500$  GeV and  $\sim 2500$  GeV, respectively. In these third family sleptonic planes, we see that the  $B_d \rightarrow K^* \mu^+ \mu^-$  constraints are super-imposed over the  $g_\mu - 2$  allowed region for heavier sleptons. So we can have heavy third family sfermions, which are required for the Higgs mass correction, and are compatible with  $g_\mu - 2$  and all other collider bounds.

In Fig. 5, we show that for  $m_{H_d}/m_{H_u}=1$ , we get data consistent with both the  $g_\mu - 2$  and  $B \rightarrow K^* \mu^+ \mu^-$  constraints. So we next do a systematic analysis of the NUHM-I based sMSSM model in which  $m_{H_u} = m_{H_d}$  but we still retain the splitting between the 1<sup>st</sup>/2<sup>nd</sup> and 3<sup>rd</sup> generation scalars.

## 4.2 sMSSM with NUHM-I

In the NUHM-I model, we have one parameter( $m_{10}$ ) to replace both  $m_{H_u}$  and  $m_{H_d}$ . One would expect this model to be slightly more constrained than the one discussed previously. In Fig. 6, we show comparison of 1<sup>st</sup> two families sfermions masses verses third family sfermions mass. We can see that for lighter  $m_{1,2}$ , the ratio  $m_3/m_{1,2}$  is large  $\sim 10$  which is lower than NUHM-II case (where it is 16). For higher  $m_{1,2}$  i.e.  $m_{1,2} \simeq 450$  GeV, this ratio decreases to 5 (as opposed to 6 in the NUHM-II case). While this seems contradictory, this is a result of amassing roughly the same number of data points for the two models and is to be treated just as a numerical

<sup>1</sup>We provide an example of the  $\tilde{\nu}_\mu$  and  $\tilde{\mu}_R$  co-annihilation with the corresponding relic densities in Table 1.

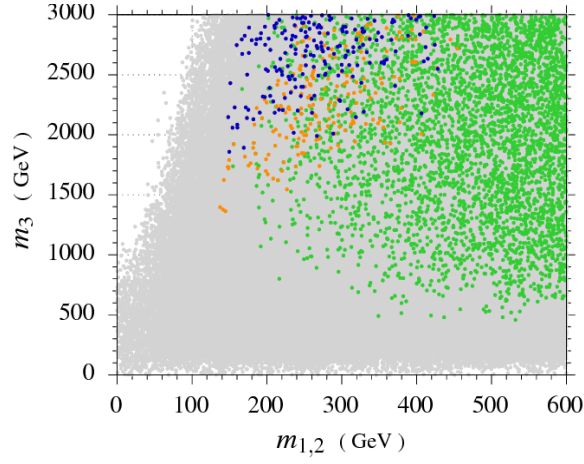


**Fig. 6.** Plot in  $m_3$ - $m_{1,2}$  plane. Color coding is same as in Fig. 1

anomaly in the results. Certainly, the NUHM-I parameter space is a subset of the NUHM-II one and the former should be more restrictive than the latter. In Fig. 7 we show plots in the  $\Delta a_\mu$  -  $m_{\tilde{\mu}_R}$ ,  $\Delta a_\mu$  -  $\tan \beta$ ,  $m_{\tilde{\mu}_R}$  -  $m_{\tilde{\chi}_1^0}$  and  $m_{\tilde{\nu}_\mu}$  -  $m_{\tilde{\chi}_1^0}$  planes. In the  $\Delta a_\mu$  -  $m_{\tilde{\mu}_R}$  plane the lower limit on  $m_{\tilde{\mu}_R}$  is same as in NUHM-II *i.e.* 200 GeV but the upper bound is decreased by a 100 GeV. The  $\Delta a_\mu$  -  $\tan \beta$  plane shows that the upper limit on  $\tan \beta$  is 52 which is less than the upper limit in NUHM-II ( $\sim 60$ ). In the  $m_{\tilde{\mu}_R}$  -  $m_{\tilde{\chi}_1^0}$  plane we can see that the upper bound on

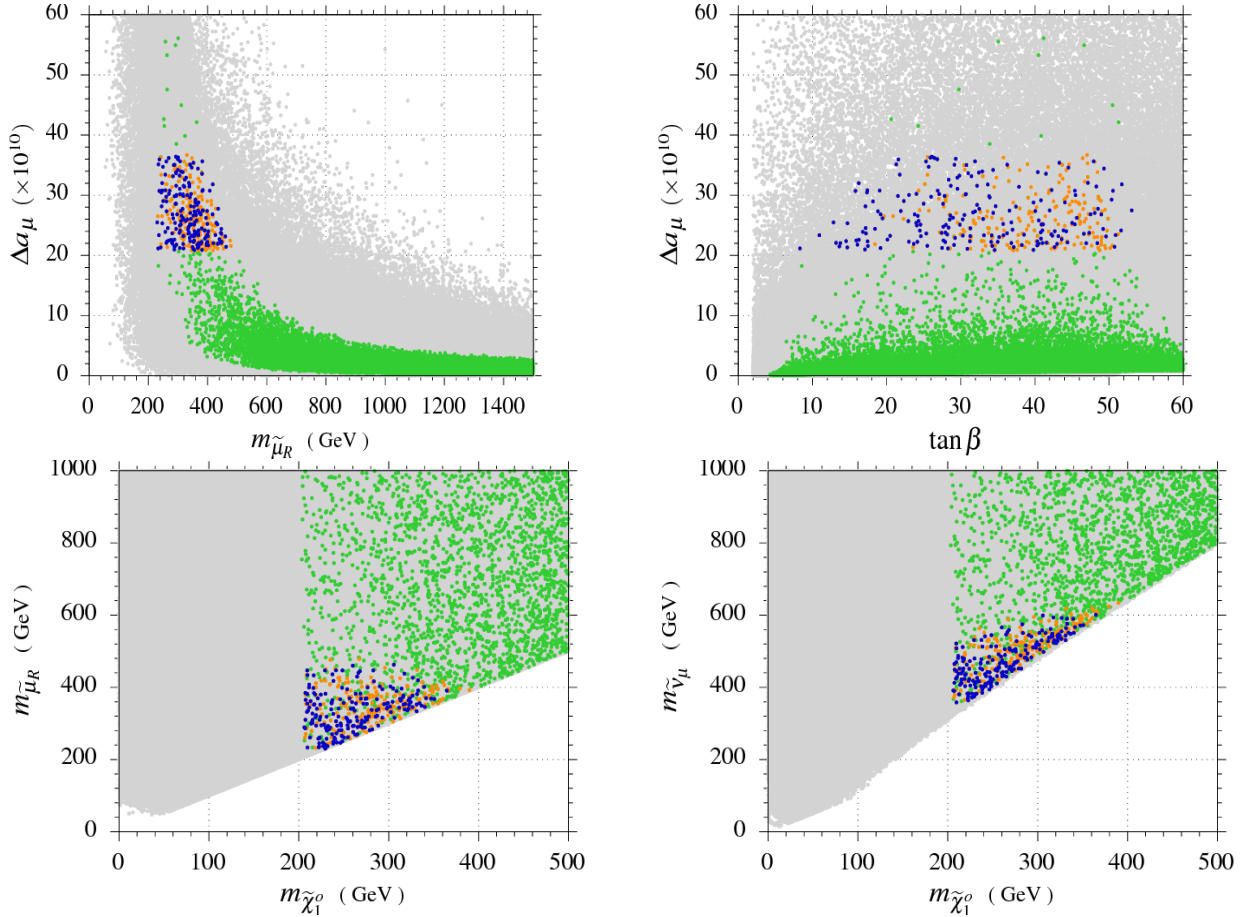


**Fig. 7.** Plots in  $\Delta a_\mu$  vs  $m_{\tilde{\mu}_R}$ ,  $\Delta a_\mu$  vs  $\tan \beta$ ,  $m_{\tilde{\mu}_R}$  vs  $m_{\tilde{\chi}_1^0}$  and  $m_{\tilde{\nu}_\mu}$  vs  $m_{\tilde{\chi}_1^0}$  planes. Color coding is the same as in Fig. 1.

$m_{\tilde{\chi}_1^0}$  has been slightly modified to 400 GeV, which was previously 420 GeV for NUHM-II as given in Fig. 4. We, however, do see co-annihilation compatible with  $g_\mu - 2$  and  $B_d \rightarrow K^* \mu^+ \mu^-$  constraints as in the previous case.

Significantly, in the  $m_{\tilde{\nu}_\mu} - m_{\tilde{\chi}_1^0}$  plane we find no co-annihilation as opposed to our plot for NUHM-II in Fig. 4. We can further see that the upper bound on the super-partner of  $\nu_\mu$  is  $\sim 600$  GeV from all constraints *i.e.* a reduction of nearly 50 GeV from our result for NUHM-II.

In Table 1 we show two points in the parameter space that are consistent with the observed dark matter relic density [42] in addition to all the other bounds considered. The first point is taken from the NUHM-II based sMSSM model and provides an example of  $\tilde{\nu}_\mu$  coannihilation. The second one is taken from the NUHM-I inspired sMSSM model and shows  $\tilde{\mu}_R$  coannihilation.

$m_{1,2}$	$m_3$	$M_{1/2}$	$A_0$	$\tan \beta$	$m_{H_u}$	$m_{H_d}$	$m_{\tilde{\nu}_\mu}$	$m_{\tilde{\mu}_R}$	$m_{\tilde{\chi}_1^0}$	$\Omega h^2$
46	2814	778	-4828	46	2639	1299	341	574	338	0.10
203	2867	737	-4730	47	1067	1067	512	322	320	0.10

Table 1: Demonstration of the possibility of getting the correct dark matter relic density for the two co-annihilation scenarios,  $\tilde{\nu}_\mu$  co-annihilation for NUHM-II inspired sMSSM (1<sup>st</sup> row) and  $\tilde{\mu}_R$  co-annihilation for NUHM-I inspired sMSSM (2<sup>nd</sup> row). All masses are in GeV.

## 5 Conclusion

We have investigated the sparticle spectrum of the flavor symmetry based Minimal Supersymmetric Standard Model (sMSSM) which is distinguished as having the third generation scalar mass parameter different from the first two. This splitting allows us to simultaneously satisfy constraints from B physics and direct mass bounds that require a heavy SUSY spectrum and the muon  $g_\mu - 2$  constraint that favors a lighter SUSY spectrum. We have provided the allowed mass ranges which are compatible with the constraints from branching ratios of radiative and pure leptonic decays  $b \rightarrow s\gamma$ ,  $B_s \rightarrow \mu^+ \mu^-$  and  $B_u \rightarrow \tau \nu_\tau$ , respectively, as well as the sparticle and gluino mass constraints, the Higgs mass constraint and the constraints from  $B_d \rightarrow K^* \mu^+ \mu^-$ . In our analysis, we have used the latest experimental data available from the LHCb, the Muon  $g - 2$  Experiment and the ATLAS and CMS collaborations.

We show that the sMSSM with both universal and non-universal Higgs mass parameters ( $m_{H_{u,d}}$ ) we are able to satisfy all the known experimental bounds and explain the Standard Model  $g_\mu - 2$  anomaly. We also show that this model can provide a dark matter candidate, which in the non-universal Higgs scenario may belong to the smuon or muon neutrino coannihilation regions. In the scenario with  $m_{H_u} = m_{H_d}$ , however, only the smuon coannihilation region is allowed by the other constraints.

We have seen that the allowed range of  $m_{\tilde{\chi}_1^0}$  is from 200 GeV to 420 GeV. We, furthermore, show that the upper limits on the stop and gluino masses are 1850 GeV and 2100 GeV respectively.

## Acknowledgments

We thank Ilia Gogoladze and Ali Paracha for useful discussions. We acknowledge the use of super-computing facility at Research Centre for Modeling and Simulations (RCMS) at National University of Sciences and Technology (NUST), Islamabad, Pakistan for the work carried out and thank the same.

# References

- [1] T. Hurth, Nucl. Phys. Proc. Suppl. **170**, 185 (2007).
- [2] A. Falkowski, M. Nardecchia and R. Ziegler, JHEP **1511**, 173 (2015).
- [3] A. Arbey, M. Battaglia, F. Mahmoudi and D. Martinez Santos, Phys. Rev. D **87**, no. 3, 035026 (2013).
- [4] A. Anandakrishnan, B. C. Bryant and S. Raby, Phys. Rev. D **90**, no. 1, 015030 (2014).
- [5] M. Misiak, S. Pokorski and J. Rosiek, Adv. Ser. Direct. High Energy Phys. **15**, 795 (1998).
- [6] A. Arbey, M. Battaglia, A. Djouadi and F. Mahmoudi, Phys. Lett. B **720**, 153 (2013).
- [7] J. Ellis, PoS Beauty **2014**, 056 (2015).
- [8] O. Buchmueller *et al.*, Eur. Phys. J. C **74**, no. 12, 3212 (2014)
- [9] K. De Causmaecker, B. Fuks, B. Herrmann, F. Mahmoudi, B. O’Leary, W. Porod, S. Sekmen and N. Strobbe, JHEP **1511**, 125 (2015).
- [10] F. Domingo and U. Ellwanger, JHEP **0712**, 090 (2007); H. Baer, M. Brhlik, D. Castano and X. Tata, Phys. Rev. D **58**, 015007 (1998); R. L. Arnowitt, B. Dutta, T. Kamon and M. Tanaka, Phys. Lett. B **538**, 121 (2002); D. Feldman, Z. Liu and P. Nath, Phys. Rev. D **81**, 117701 (2010); J. Kawamura and Y. Omura, Phys. Rev. D **93**, 055019 (2016); K. De Causmaecker, B. Fuks, B. Herrmann, F. Mahmoudi, B. O’Leary, W. Porod, S. Sekmen and N. Strobbe, JHEP **1511**, 125 (2015).
- [11] R. Aaij *et al.* [LHCb Collaboration], JHEP **1308**, 131 (2013).
- [12] W. Gohn, M. Davier, A. Hoecker, B. Malaescu and Z. Zhang, Eur. Phys. J. C **71**, 1515 (2011) [Erratum-ibid. C **72**, 1874 (2012)]; M. Benayoun, P. David, L. DelBuono and F. Jegerlehner, Eur. Phys. J. C **73**, 2453 (2013).
- [13] Muon g-2 Collaboration, Phys. Rev. D **73**, 072003 (2006).
- [14] M. A. Ajaib, B. Dutta, T. Ghosh, I. Gogoladze and Q. Shafi, “Neutralinos and sleptons at the LHC in light of muon  $(g - 2)_\mu$ ,” Phys. Rev. D **92**, 075033 (2015).
- [15] G. Aad *et al.* [ATLAS Collaboration], Phys. Lett. B **716**, 1 (2012).
- [16] S. Chatrchyan *et al.* [CMS Collaboration], Phys. Lett. B **716**, 30 (2012).
- [17] S. Heinemeyer, O. Stal and G. Weiglein, Phys. Lett. B **710**, 201 (2012); A. Arbey, M. Battaglia, A. Djouadi, F. Mahmoudi and J. Quevillon, Phys. Lett. B **708**, 162 (2012).
- [18] See for instance A. Arbey, M. Battaglia, A. Djouadi, F. Mahmoudi and J. Quevillon, Phys. Lett. B **708**, 162 (2012); H. Baer, V. Barger and A. Mustafayev, Phys. Rev. D **85**, 075010 (2012).
- [19] See for instance P. Draper, P. Meade, M. Reece and D. Shih, Phys. Rev. D **85**, 095007 (2012); M. A. Ajaib, I. Gogoladze, F. Nasir and Q. Shafi, Phys. Lett. B **713**, 462 (2012).
- [20] See for instance B. Zhu, R. Ding and T. Li, arXiv:1610.09840 [hep-ph] and references therein.

- [21] K. S. Babu, I. Gogoladze, Q. Shafi and C. S. n, Phys. Rev. D **90**, no. 11, 116002 (2014).
- [22] K. S. Babu, I. Gogoladze, S. Raza and Q. Shafi, Phys. Rev. D **90**, no. 5, 056001 (2014).
- [23] J. R. Ellis, S. Heinemeyer, K. A. Olive, A. M. Weber and G. Weiglein, JHEP **0708**, 083 (2007).
- [24] W. Altmannshofer, A. J. Buras, S. Gori, P. Paradisi and D. M. Straub, Nucl. Phys. B **830**, 17 (2010).
- [25] A. Bartl, T. Gajdosik, E. Lunghi, A. Masiero, W. Porod, H. Stremnitzer and O. Vives, PoS HEP **2001**, 169 (2001).
- [26] F. Mahmoudi, arXiv:1205.3099 [hep-ph].
- [27] F. Mahmoudi, S. Neshatpour and J. Orloff, JHEP **1208**, 092 (2012).
- [28] F. Mahmoudi, Int. J. Mod. Phys. A **29**, 1444012 (2014).
- [29] A. J. Buras, hep-ph/9806471.
- [30] F. Mahmoudi, S. Neshatpour and J. Virto, Eur. Phys. J. C **74**, no. 6, 2927 (2014).
- [31] J. Matias, F. Mescia, M. Ramon and J. Virto, JHEP **1204**, 104 (2012).
- [32] T. Hurth, F. Mahmoudi and S. Neshatpour, Nucl. Phys. B **909**, 737 (2016).
- [33] S. Descotes-Genon, J. Matias and J. Virto, PoS EPS **-HEP2013**, 361 (2013).
- [34] Y. Kawamura, H. Murayama and M. Yamaguchi, Phys. Rev. D **51**, 1337 (1995).
- [35] B.C. Allanach, Comput. Phys. Commun. **143** (2002) 305-331.
- [36] J. R. Ellis, T. Falk, K. A. Olive and Y. Santoso, Nucl. Phys. B **652** (2003) 259.
- [37] P. Z. Skands *et al.*, JHEP **0407**, 036 (2004).
- [38] F. Mahmoudi, Comput. Phys. Commun. **180**, 1579 (2009).
- [39] G. Aad *et al.* [ATLAS Collaboration], Phys. Rev. D **87**, no. 1, 012008 (2013).
- [40] A. Cervelli [ATLAS and CMS Collaborations], PoS EPS **-HEP2015**, 157 (2015).
- [41] G. W. Bennett *et al.* [Muon g-2 Collaboration], Phys. Rev. D **73**, 072003 (2006).
- [42] G. Hinshaw *et al.* [WMAP Collaboration], Astrophys. J. Suppl. **208**, 19 (2013).